




**Theoretical design of ellipsoidal nodal surface semimetals via hypervalent hydrides at high pressure**Zihan Zhang,<sup>1</sup> Mingfeng Zhu,<sup>1</sup> Hao Song ,<sup>2</sup> Feng Liu ,<sup>2</sup> Bartomeu Monserrat,<sup>3,4,\*</sup> Chris J. Pickard,<sup>3,5</sup> Defang Duan ,<sup>1,†</sup> and Tian Cui<sup>2,1,‡</sup><sup>1</sup>State Key Laboratory of Superhard Materials, College of Physics, Jilin University, Changchun 130012, China<sup>2</sup>Institute of High Pressure Physics, School of Physical Science and Technology, Ningbo University, Ningbo 315211, People's Republic of China<sup>3</sup>Department of Materials Science & Metallurgy, University of Cambridge, 27 Charles Babbage Road, Cambridge CB3 0FS, United Kingdom<sup>4</sup>Cavendish Laboratory, University of Cambridge, J. J. Thomson Avenue, Cambridge CB3 0HE, United Kingdom<sup>5</sup>Advanced Institute for Materials Research, Tohoku University 2-1-1 Katahira, Aoba, Sendai 980-8577, Japan

(Received 7 January 2021; revised 22 September 2023; accepted 18 October 2023; published 13 November 2023)

Topological band theory has emerged as a powerful framework to classify and understand the electronic properties of materials. Topological semimetals, which have protected band crossings near the Fermi level and include Dirac and Weyl points, lines, or surfaces, generally remain uncommon. Hypervalent compounds exhibit tunable highly degenerate nonbonding states driving band crossings, so they could provide an effective platform to explore topological semimetallic phases. Here, we identify the topology of the electronic structure of hypervalent hydrides  $A_2BH_6$  at ambient pressure and high pressure, and describe the microscopic origin of topological states via hydrogen nonbonding states. Importantly, we discover an ellipsoidal nodal surface, a hitherto unrecognized type of fermionic excitation, in  $Mg_2BeH_6$  with space group  $Fm\bar{3}m$ . The nodal surface electrons couple strongly to phonons, causing a lattice instability that drives the system towards a charge density wave phase that competes with the topological nodal surface phase, with pressure providing a control parameter. Additionally, in the nodal surface phase we predict superconductivity with a critical temperature of 20 K. We anticipate our work will encourage materials realizations of topological phases and help rationalize high pressure experiments using ideas from topological theory.

DOI: [10.1103/PhysRevB.108.205119](https://doi.org/10.1103/PhysRevB.108.205119)**I. INTRODUCTION**

Three-dimensional Dirac (Weyl) semimetals are a type of quantum matter hosting topology protected four-band (two-band) crossings close to the Fermi level at isolated points [1,2], lines [3,4], or even surfaces [5,6] in the Brillouin zone. The associated fermionic quasiparticles in condensed matter systems, many of which have no analogs in high-energy theories [3,7], drive physical phenomena [8]. For example, axions as elementary particles are yet to be observed in nature, but can emerge as collective electronic excitations in Weyl semimetals, such as  $(TaSe_4)_2I$ , in which they drive the structure into a charge density wave phase [9].

Although there are multiple examples of point and line semimetals, nodal-surface semimetals remain rare.

Additionally, most known nodal surface semimetals have the nodal surface nearly parallel to boundary planes of the Brillouin zone [5,6,10–12], while alternative configurations such as nodal spheres are only “pseudonodal” surfaces because they are gapped by spin-orbit coupling. The more abundant nodal line semimetals exist in a wider variety of configurations, including nodal rings [13], nodal chains [3], and nodal nets [4]. This prompts the questions of whether there are yet to be uncovered configurations for nodal surfaces, driving widespread attention in the chemistry and materials communities to design topological nodal surface semimetals. To address this challenge, we propose a general strategy to design classes of topological semimetals using hypervalent structures and pressure, and we successfully uncover a different type of ellipsoidal nodal-surface semimetal.

The crossing of energy bands is a common phenomenon which controls properties of materials such as their metallic and topological states [14,15]. Two methods have been traditionally pursued to promote band crossings: mechanical external pressure [16] and chemical internal pressure [17]. Indeed, these have been fundamental to drive the overlap of energy bands underpinning the recently discovered metallic and superconducting high pressure hydrides [18,19]. Similar strategies hold great promise to explore the promotion of topological semimetals by driving band overlap, even in simple light elemental substances like hydrogen [20] and lithium [13].

\*Corresponding author: [bm418@cam.ac.uk](mailto:bm418@cam.ac.uk)†Corresponding author: [duandf@jlu.edu.cn](mailto:duandf@jlu.edu.cn)‡Corresponding author: [cuitian@nbu.edu.cn](mailto:cuitian@nbu.edu.cn); [cuitian@jlu.edu.cn](mailto:cuitian@jlu.edu.cn)

TABLE I. Topological Dirac phase and structural stability of all  $A_2BH_6$  hydrides studied in this work at pressures of 0 and 300 GPa.

Hydrides		Properties			
$A_2BH_6$		0 GPa		300 GPa	
A/electronegativity	B/electronegativity	Topology	Stability	Topology	Stability
Ba/0.97	Be/1.47	none	stable	type I	unstable
Ca/1.04	Be/1.47	none	stable	type II	stable
Mg/1.23	Be/1.47	type I	unstable	type I	stable
Sr/0.99	Be/1.47	none	stable	none	stable
Ba/0.97	Cu/1.75	type III	stable	type III	unstable
Ca/1.04	Cu/1.75	type III	stable	type III	unstable
Mg/1.23	Cu/1.75	type III	unstable	type III	stable
Sr/0.99	Cu/1.75	type III	stable	type III	stable
Ba/0.97	Zn/1.66	none	stable	type II	stable
Ca/1.04	Zn/1.66	none	stable	type II	stable
Mg/1.23	Zn/1.66	type I	unstable	type I	stable
Sr/0.99	Zn/1.66	none	stable	type II	stable

Motivated by these observations, hypervalent compounds, which are common at high pressure [21,22], have been identified as a key family for discovering and understanding topological materials [23,24]. For example, the axion insulator  $(\text{TaSe}_4)_2\text{I}$  [9], in which a charge density wave (CDW)

gaps the Weyl points, is a hypervalent material with partially occupied orbitals arising from the anion unit  $[\text{ISe}_4]^{5-}$ , which exhibits a similar valence electronic structure and square plane crystal structure to that of the classical hypervalent molecule  $\text{XeF}_4$  with two three-center-four-electron ( $3c - 4e$ ) bonds. Simultaneously, polyhydrides under high pressure such as  $\text{H}_3\text{S}$  [18],  $\text{LaH}_{10}$  [25] and  $\text{CeH}_9$  [26], which are high temperature superconductors [18,27–29], always exhibit band crossings around the Fermi level, suggesting their superconductivity could coexist with topological states.

In this work we explore hypervalent hydrides under pressure as a platform to study the role of hypervalent orbitals in driving potentially simultaneous topological states, superconductivity, and CDWs. In recent years, many hydrogen-rich compounds have been discovered from high pressure and high temperature synthesis and theoretical predictions, with examples including  $\text{K}_2\text{SiH}_6$  [21],  $\text{Na}_3\text{FeH}_7$ , and  $\text{Na}_3\text{CoH}_6$  [30]. We chose hypervalent hydrides  $A_2[\text{BH}_6]$ , crystallizing in the cubic  $\text{K}_2\text{SiH}_6$   $Fm\bar{3}m$  structure, as the template to explore these physical phenomena in this work. We find that Dirac states in these hydrides can be tuned by the number of valence electrons, the electronegativity of the component elements, and pressure. As a result, we discover a topological state, an ellipsoidal nodal surface semimetal, and propose its high-pressure realization in  $\text{Mg}_2\text{BeH}_6$ . Additionally, we find a strong coupling between the ellipsoidal nodal surface electrons and the phonons in  $\text{Mg}_2\text{BeH}_6$ , driving a CDW phase which gaps the Dirac nodal surface in a similar manner to that observed in the axion insulator  $(\text{TaSe}_4)_2\text{I}$ .

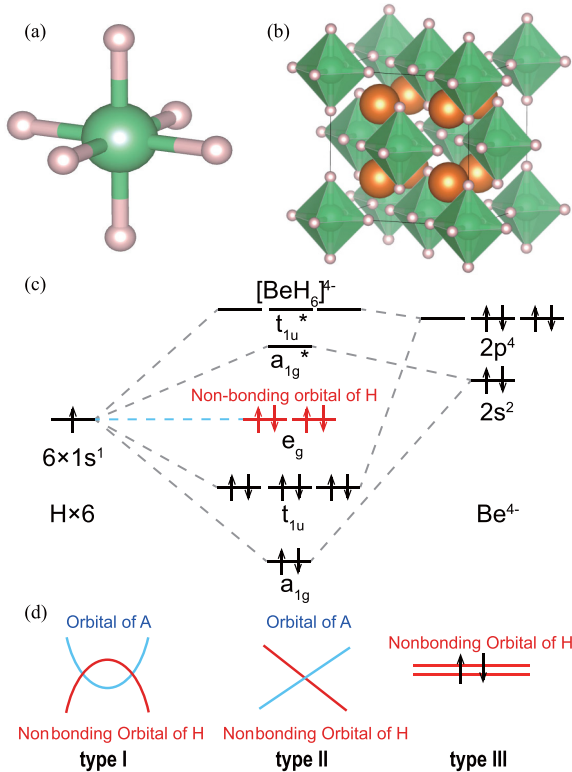


FIG. 1. Structure, molecular orbitals, and possible topological states of hypervalent unit  $[\text{BeH}_6]^{4-}$  in hydrides  $\text{Mg}_2\text{BeH}_6$  ( $Fm\bar{3}m$ ). (a) Hypervalent unit  $[\text{BeH}_6]^{4-}$ . (b) The crystal structure of  $\text{Mg}_2\text{BeH}_6$ . The anion coordination complexes  $[\text{BeH}_6]^{4-}$  are shown as green octahedra and the Mg ions as orange atoms. (c) Molecular orbitals of the three-center-four-electron hypervalent unit  $[\text{BeH}_6]^{4-}$ . (d) Three types of Dirac states and orbitals in  $\text{Mg}_2\text{BeH}_6$ .

### A. Hypervalent $A_2BH_6$ hydrides: Crystal structure and electronic structure

Dirac semimetals appear in compounds with high symmetry crystal structures that can host multiple band degeneracies [31]. Of these, those with light elements and correspondingly weak spin-orbit coupling dominate, as spin-orbit coupling can gap band degeneracies [12,13,32]. Hypervalent compounds with  $3c - 4e$  bonds always exhibit high symmetry structures, for example the crystal structure of the  $\text{SF}_6$  family. However,

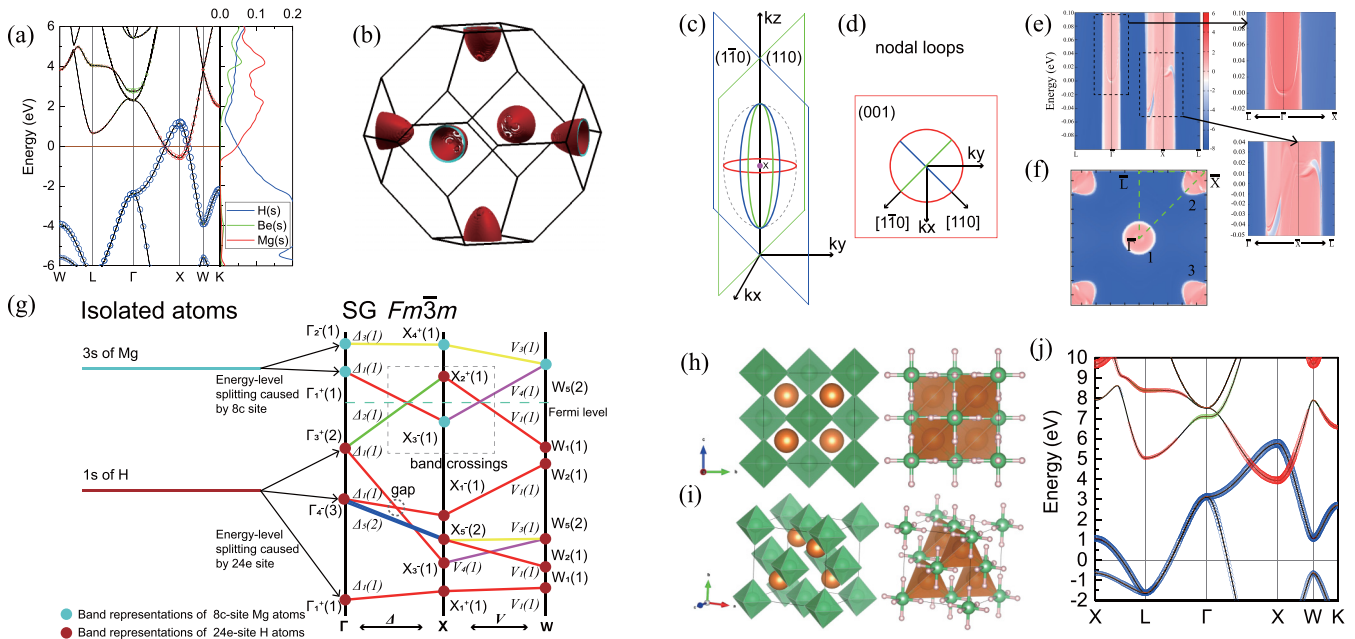


FIG. 2. The electronic structure and topological properties of  $\text{Mg}_2\text{BeH}_6$  ( $Fm\bar{3}m$ ). (a) Band structure of  $\text{Mg}_2\text{BeH}_6$ , in which band crossings consist of different orbitals from different atoms. (b) The ellipsoidal Fermi surface of  $\text{Mg}_2\text{BeH}_6$ . (c),(d) The mirror-symmetry-protected nodal loops appear in  $\text{Mg}_2\text{BeH}_6$  ( $Fm\bar{3}m$ ) with their mirror planes ( $1\bar{1}0$ ),  $(110)$ , and  $(001)$ , and the other points, which are on the nodal loops but not on these nodal loops, are accidental degeneracy or small gapped ( $\sim 1$  meV). (e) Density of states of the  $(001)$  surface Brillouin zone. The flat bands of each ellipsoidal nodal surface are near the Fermi level. (f) Density of states at the Fermi level in the  $(001)$  surface Brillouin zone. The shape of density red block is the projection of ellipsoids with different direction (labels 1–3). (g) Orbital character and band representations around nodal surface at high symmetry points and along high symmetry lines of Mg and H atoms in  $\text{Mg}_2\text{BeH}_6$  ( $Fm\bar{3}m$ ). (h),(i) The crystal structure of the  $\text{MgBeH}_6$ . (j) The band structure of  $\text{MgBeH}_6$ . The band crossings almost do not change, because mirror symmetry of planes  $(1\bar{1}0)$  and  $(110)$  do not change, and the Fermi level decreases with absence of a Mg atom per primitive cell.

these compounds traditionally have large band gaps driven by the large electronegativity of coordinate elements such as F and Cl, and therefore make poor candidates for Dirac semimetals. The recent synthesis of hypervalent high pressure hydride,  $\text{K}_2\text{SiH}_6$  with space group  $Fm\bar{3}m$ , provides a H-based hypervalent compound family [21,22], exhibiting much lower electronegativities and therefore the possibility of metallization. The family prototype is  $\text{A}_2[\text{BH}_6]$ , with a  $\text{A}^{2+}$  cation and a  $[\text{BH}_6]^{4-}$  unit, and there exist multiple predictions of such hydrides stable at ambient pressure. In these compounds, it is possible to understand how the  $[\text{BH}_6]^{4-}$  octahedra can drive a Dirac semimetallic phase with two independent mechanisms: (i) the nonbonding state of H itself is degenerate as shown in Figs. 1(a) and 1(b); (ii) although  $[\text{BH}_6]^{4-}$  octahedra have the same valence electrons as  $\text{SF}_6$ , H exhibits much lower electronegativity than F, so it is possible to find overlap between occupied nonbonding orbitals of H and unoccupied atomic orbitals in the crystal constituted by  $[\text{BH}_6]^{4-}$  octahedra.

In this work, we explore the band structure topology in high symmetry hydrides  $\text{A}_2[\text{BH}_6]$  ( $\text{A} = \text{Mg}^{2+}$ ,  $\text{Ca}^{2+}$ ,  $\text{Sr}^{2+}$ ,  $\text{Ba}^{2+}$ , and  $\text{B} = \text{Be}^{2+}$ ,  $\text{Zn}^{2+}$ ,  $\text{Cu}^{2+}$ ) made of light elements. The combination of high symmetry and weak SOC should provide a fertile playground for discovering Dirac semimetallic phases. Furthermore, given the experimental discovery of this family at high pressure, we explore these compounds at both ambient pressure and 300 GPa. Our main results are

summarized in Table I for all considered hydrides. We find three different types of Dirac semimetal states around the Fermi level. As schematically depicted in Fig. 1(d), type I and II semimetals involve crossings of metal A states with nonbonding H states, while type III semimetals involve degeneracies amongst the nonbonding H states only.

The type of Dirac states that appears in each compound strongly depends on the electronegativity of the constituents, which controls the relative position of the energy of the orbitals. In particular, type III states only emerge in semimetals with  $[\text{CuH}_6]^{4-}$ , because Cu has the highest electronegativity compared to Be and Zn, raising the flat bands of degenerate nonbonding orbitals close to the Fermi level.

Pressure also plays an important role in determining the type of Dirac states present in each compound. Type I states at ambient pressure are only present in hydrides with Mg because its low electronegativity compared to Ca, Sr, and Ba causes smaller band gaps and leads to band crossings between orbitals of Mg and nonbonding orbitals. But most importantly, pressure reduces band gaps and drives band crossings, and most trivial hydrides at ambient pressure become topological at 300 GPa.

We also explore the structural stability of the studied hydrides by calculating their phonon dispersion, and summarize our results in Table I. Of all compounds studied, we identify  $\text{Mg}_2\text{BeH}_6$  as an interesting material for further investigation. It is a type I Dirac semimetal that hosts a type of ellipsoidal

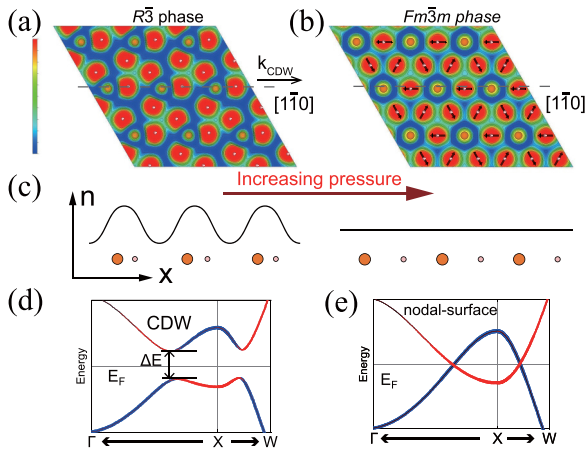


FIG. 3. Pressure-induced transformation from a CDW phase ( $R\bar{3}$ ) to a nodal-surface phase ( $Fm\bar{3}m$ ) in  $Mg_2BeH_6$ . (a),(b) The (111) surface ELF of the  $R\bar{3}$  and  $Fm\bar{3}m$  phases. A CDW exists along the gray dotted line in the  $R\bar{3}$  phase, stable at pressures below 300 GPa. (c) Schematic anti-Peierls-like transition induced by increasing pressure from the  $R\bar{3}$  phase to the  $Fm\bar{3}m$  phase. (d),(e) The band structures of the CDW phase and the semimetal phase.

nodal surface. Additionally, it is dynamically unstable at ambient conditions but stabilized by pressure, suggesting that it may host a CDW phase as that observed in other related compounds such as  $TaSe_2$  [33], in which pressure weakens the CDW phase and enhances the superconducting phase. The coexistence of topological semimetallic electrons and a CDW also suggests there may be interesting coupling between electrons and phonons in this compound.

### B. Ellipsoidal nodal surface in $Mg_2BeH_6$

The band structure and Fermi surface of  $Mg_2BeH_6$  in the high pressure  $Fm\bar{3}m$  phase are shown in Figs. 2(a) and 2(b), respectively, exhibiting a rare ellipsoidal nodal surface. The corresponding surface states form flat bands, and are shown in Figs. 2(e) and 2(f). The ellipsoidal nodal surfaces around the high symmetry  $X$  points arise from the band overlap between an orbital from the Mg atoms at the  $8c$  sites and a nonbonding orbital from the hypervalent  $[BeH_6]^{4-}$  unit [see Fig. 2(a)]. The location of the band crossings implies that the representations of the point group  $D_{4h}$  [31,34,35] of the  $X$  points plays an important role in the emergence of the nodal surface. In the subsequent analysis, we neglect SOC because it is extremely weak in  $Mg_2BeH_6$ . The band representations of H [Fig. 2(g)] at the  $\Gamma$  point agree well with the molecular orbital of the hypervalent unit  $[BeH_6]^{4-}$  [Fig. 1(c)]: from low energy to high energy the band degeneracies from hydrogen are 1, 3, and 2 at the  $\Gamma$  point. The two band representations of the nodal surface states at the  $X$  point are  $X_3^-(1)$  and  $X_2^+(1)$ , as shown in Fig. 2(g). Additionally, the two bands forming the nodal surface have different mirror-symmetry eigenvalues on the mirror planes  $(1\bar{1}0)$ ,  $(110)$ , and  $(001)$ , so a nodal loop appears on each plane protected by mirror symmetry. Because  $Mg_2BeH_6$  has cubic  $Fm\bar{3}m$  symmetry, the  $X$  points exhibit all three mirror planes and the three nodal loops cross, forming the backbone [31] of an ellipsoid. We find that the degeneracy

on the nodal loops, which is enforced by symmetry, extends as an accidental degeneracy to the entire ellipsoid, forming an ellipsoidal nodal surface. Accidental degeneracies are present at low symmetry  $k$  points in many materials [36], and although they tend to become gapped by SOC [36], the SOC strength of  $Mg_2BeH_6$  is too weak to gap the band crossings significantly (gaps are less than 1 meV). As a result, we propose  $Mg_2BeH_6$  as a candidate ellipsoidal nodal surface semimetal.

To understand the origin of the nodal surface in  $Mg_2BeH_6$ , we note that nodal surfaces are present in systems with chiral symmetry [11]. The antiferrotype structure of  $Mg_2BeH_6$  is not bipartite because the  $[BeH_6]^{4-}$  anion octahedra and the pair of Mg cations are not identical and do not form equivalent sublattices. Additionally, the band crossings of  $Mg_2BeH_6$  involve the  $1s$  orbital of H atoms and  $3s$  orbital of Mg atoms. However, although  $Mg_2BeH_6$  does not have chiral symmetry, the effective Hamiltonian describing the low-energy part of the spectrum of  $Mg_2BeH_6$  does have chiral symmetry [5], thus driving the existence of the nodal surface [see the “topological charge of  $Mg_2BeH_6$  ( $Fm\bar{3}m$ )” section in the Supplemental Material [37]].

Crystals with chiral symmetry are generally bipartite with half-filled even-numbered bands which host band crossings at the Fermi level, with graphene being a well-known example. The mechanism driving the nodal surface in  $Mg_2BeH_6$  is the overlap of bands from Mg atoms and  $BeH_6$  hypervalent units, which mainly depends on the electronegativity rather than on half-filled even-numbered bands. Therefore, the ellipsoidal nodal surface does not depend on chiral symmetry.

To further explore the role played by Mg atoms in the  $8c$  site of the  $Fm\bar{3}m$  space group, we perform a computational experiment. We remove a Mg atom from the primitive cell to get a hypothetical  $MgBeH_6$  compound, with a structure that is bipartite and similar to that of nodal chain metals [3], with the sublattices formed by the Mg atoms and the  $[BeH_6]^{4-}$

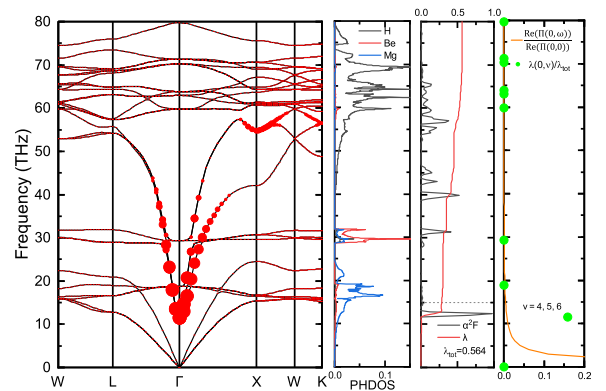


FIG. 4. The phonon dispersion, density response function of frequency of  $Mg_2BeH_6$  ( $Fm\bar{3}m$ ) at 300 GPa. From left to right, phonon dispersion relation with phonon linewidths, projected phonon densities of states (PHDOS), and spectral function  $\alpha^2 F$  with electron-phonon coupling strength  $\lambda$  integral of frequency. The last graph shows that proportion of the  $(q, \nu)$ -resolved  $\lambda$  (the number denotes the corresponding vibration mode  $\nu$ ) in total  $\lambda$  at  $\Gamma$  point and the frequency dependence of the real part of relative response function  $Re(\Pi(\omega, \mathbf{q}))/Re(\Pi(0, 0))$ .

octahedra, as shown in Figs. 2(h) and 2(i). This hypothetical hydride  $\text{MgBeH}_6$  has topological Dirac ellipsoidal nodal surfaces around 4.5 eV above the Fermi energy, with the shift in energy caused by the absence of two electrons from the Mg atom per primitive cell that has been removed. Although the chiral symmetry of  $\text{Mg}_2\text{BeH}_6$  is broken by the extra Mg atoms, the nodal surfaces survive with nodal-loop-backbones protected by mirror planes  $(\bar{1}\bar{1}0)$  and  $(110)$ . As a side note, this shows that the Mg cations not only take part in establishing the chiral symmetry, but also contribute free electrons to raise the Fermi level to an energy close to that of nodal surface.

### C. CDW, response function, and nodal-surface-phonon coupling

Semimetals often undergo a charge density wave instability that gaps the band crossings, and this is indeed the case for the ellipsoidal nodal surface semimetal  $\text{Mg}_2\text{BeH}_6$ , which exhibits imaginary phonon modes at ambient conditions. Pressure can often suppress CDW instabilities, and we find that  $\text{Mg}_2\text{BeH}_6$  becomes dynamically stable at 300 GPa. These observations suggest  $\text{Mg}_2\text{BeH}_6$  may exhibit a complex structural phase diagram, and we next explore it in some detail.

Structure searching methods have been successfully used in the search for CDW phases [57]. Here, we use the *ab initio* random structure searching (AIRSS) method [38] to predict the CDW phase of cubic  $\text{Mg}_2\text{BeH}_6$ . We identify a  $R\bar{3}$  phase of stoichiometry  $\text{Mg}_2\text{BeH}_6$ , which undergoes a smooth phase transformation to the  $Fm\bar{3}m$  phase under pressure, and corresponds to the CDW phase of the ellipsoidal nodal surface as shown in Fig. 3.

The CDW gaps the band crossing around the nodal surface. As shown in Fig. 3(b), the dimerization of H atoms and Mg atoms caused by a lattice instability gaps the nodal surface at lower pressure, similar to what is observed in the axion insulator  $(\text{TaSe}_4)_2\text{I}$ . Notably, the dimerization in  $\text{Mg}_2\text{BeH}_6$  looks like a ‘‘Peierls transition,’’ but it is not a typical Peierls transition because a Peierls transition emerges with chiral symmetry and  $\text{Mg}_2\text{BeH}_6$  does not have chiral symmetry. This structural transition can be characterized by the tilting angle of the  $[\text{BeH}_6]^{4-}$  octahedra (see Fig. S15 in the Supplemental Material [37]), pushing the H atoms towards the Mg atoms and driving dimerization. Therefore, we can use the tilting angle as an order parameter to quantify the symmetry changes that occur during the phase transition between the semimetal and CDW phases. As pressure increases, the tilting angle of the  $[\text{BeH}_6]^{4-}$  octahedra decreases, and pressure eventually overcomes the instability in  $\text{Mg}_2\text{BeH}_6$ . Overall, we find that a CDW phase competes with the topological semimetallic phase, but that high pressure can help stabilize the high symmetry semimetallic phase. This pressure-driven stabilization of high symmetry phases is a common feature of coordinated compounds, with recent examples including the metallic hydrogen-rich compounds  $\text{H}_3\text{S}$  [18,27] and  $\text{LaH}_{10}$  [28,29].

It is well known that ordinary Fermi surfaces can exhibit strong electron-phonon coupling, for example resulting in the

Kohn anomaly [58] or Fermi surface nesting [59]. When the Fermi surface is a nodal surface with a linear dispersion in the normal direction, exotic electron-phonon coupling mechanisms may arise [60]. Motivated by this, we explore the role of electron-phonon coupling in the ellipsoidal nodal surface of  $\text{Mg}_2\text{BeH}_6$ .

The phonon dispersion and electron-phonon coupling strength of the  $Fm\bar{3}m$  phase calculated using DFT at 300 GPa show an abrupt softening of the optical phonon modes around the  $\Gamma$  point (Fig. 4), and below 300 GPa imaginary frequencies emerge. The calculated value of the total electron-phonon coupling strength  $\lambda$  is 0.564 (broadening  $\sigma = 0.01$ ) on the nodal surface. The mode-resolved electron-phonon coupling strength is shown on the phonon dispersion relation (Fig. 4), and the electron-phonon coupling is strongest at the  $\Gamma$  point. At the  $\Gamma$  point, the electron-phonon coupling strength  $\lambda$  ( $\sim 0.28$ ) is much larger than at any of the other 215 phonon momenta  $\mathbf{q}$  included in our calculations, and the sum over the three lowest energy optical modes at  $\Gamma$  is around 50% of the total  $\lambda$ , although the weight of the  $\Gamma$  point is only 1/216 ( $\sim 0.005$ ). The resulting superconducting critical temperature  $T_c$  is predicted to be around 20 K, which is high for Dirac semimetals.

To provide a microscopic explanation for the phonon softening driven by strong coupling to electrons as calculated by DFT, we build an effective massless Dirac quasiparticles model that includes the electronic low-energy excitations on the ellipsoidal nodal surface of  $\text{Mg}_2\text{BeH}_6$ . To derive such a model, we note that all the points on the ellipsoidal nodal surface are Dirac points whose dispersion is linear along the nodal surface normal direction (Fermi velocities), and SOC is weak in the Mg-Be-H system so it can be neglected and the resulting effective model is a two band Hamiltonian. As shown in Sec. 2.1 of the Supplemental Material [37], the low-energy Hamiltonian of the nodal surface takes the form

$$H(\mathbf{k}) = \frac{\partial E(\mathbf{k})}{\partial \bar{\mathbf{n}}} \left( \frac{k_x - k_{F_x}(\mathbf{k})}{a} \sigma_x + \frac{k_y - k_{F_y}(\mathbf{k})}{a} \sigma_y + \frac{k_z - k_{F_z}(\mathbf{k})}{b} \sigma_z \right),$$

where  $k_{F_x}(k)$ ,  $k_{F_y}(k)$ , and  $k_{F_z}(k)$  are the components of the Fermi vector  $\mathbf{k}_F$  along the  $x$ ,  $y$ , and  $z$  axis,  $a$ ,  $b$ ,  $k_{z_0}$  are the semimajor axis, semiminor axis, and center of our ellipsoidal Hamiltonian model, and  $k_{z_0} = \overline{\Gamma X}$  (Fig. 1). Then we parametrize the model using the DFT band structure, with  $a$  and  $b$  parametrized from the band crossings along  $\overline{\Gamma X}$  and  $\overline{XW}$  in the first Brillouin zone, and the slope  $\frac{\partial E(\mathbf{k})}{\partial \bar{\mathbf{n}}}$  is assumed to be constant and taken to be the average slope along the major and minor axes.

To study the interaction of phonons and Dirac nodal surface electrons, we analyze the behavior of the density response function divided into intraband and interband

excitations as follows:

$$\begin{aligned} \Pi^{00}(\omega, \mathbf{q}) = \Pi_{\text{intra}}(\omega, \mathbf{q}) + \Pi_{\text{inter}}(\omega, \mathbf{q}), \quad \Pi_{\text{intra}}(\omega, \mathbf{q}) = 2 \sum_k \Gamma_{k,\mathbf{q}}^{\text{intra}} \left[ \frac{n[E_+(k)] - n[E_+(k + \mathbf{q})]}{\hbar\omega - E_+(k + \mathbf{q}) + E_+(k) + i0^+} \right. \\ \left. + \frac{n[E_-(k)] - n[E_-(k + \mathbf{q})]}{\hbar\omega - E_-(k + \mathbf{q}) + E_-(k) + i0^+} \right], \quad \Pi_{\text{inter}}(\omega, \mathbf{q}) = 2 \sum_k \Gamma_{k,\mathbf{q}}^{\text{inter}} \left[ \frac{n[E_-(k)] - n[E_+(k + \mathbf{q})]}{\hbar\omega - E_+(k + \mathbf{q}) + E_-(k) + i0^+} \right. \\ \left. + \frac{n[E_+(k)] - n[E_-(k + \mathbf{q})]}{\hbar\omega - E_-(k + \mathbf{q}) + E_+(k) + i0^+} \right], \end{aligned}$$

where  $\Gamma_{k,\mathbf{q}}^{\text{intra}}$  and  $\Gamma_{k,\mathbf{q}}^{\text{inter}}$  are the chirality factors for the intra- and interband transitions as shown in Fig. S20 [37].

As shown in Fig. 4, the strong electron-phonon coupling associated with the three lowest energy optical modes at the  $\Gamma$  point is the result of the anomalous density response function  $\Pi(\omega, \mathbf{q})$  of the nodal surface quasiparticles [58–60]. The density response function  $\Pi(\omega, \mathbf{q})$  abruptly increases when  $\mathbf{q}$  approaches  $\Gamma$  and the frequency of the optical mode goes to 0. As a result, the ability of the electrons to screen the embedded charge suddenly decreases when  $(\omega, \mathbf{q})$  approaches  $(0, 0)$ . As shown in Fig. 4, at the  $\Gamma$  point the optical vibrational modes with lowest frequency contribute most of the electron-phonon coupling strength because the response of nodal surface excitations to low-frequency phonons is much stronger than the response to high frequency phonons, which is embodied by the infinite slope of the response function around  $\omega = 0$ . This allows us to further characterize the lattice instability of the  $Fm\bar{3}m$  phase below 300 GPa discussed above: band crossings might cause dynamical instabilities that can drive a phase transformation from semimetallic phases to gapped phases.

## II. SUMMARY

In summary, designing Dirac materials with hypervalent hydrides is shown to be an effective approach to obtaining topological states with overlapping bands from H-rich hypervalent units. We identify multiple topological states, natural or induced by pressure, in hypervalent hydrides  $A_2BH_6$ . Most interestingly, we discover an ellipsoidal nodal surface state in the  $Fm\bar{3}m$  structure of  $Mg_2BeH_6$ . We also find that this semimetallic phase competes with a CDW phase, and that pressure stabilizes the Dirac nodal surface state. Additionally, we find a relatively high superconducting critical temperature of 20 K in the Dirac semimetallic phase.

The prediction of an ellipsoidal nodal-surface state in the  $A_2BH_6$  hydrides can motivate further theoretical and experimental studies on the relationship between CDWs, Dirac

nodal surfaces, and superconductivity, especially at high pressure. Dirac materials at high pressure remain a largely unexplored arena with only a few recent examples, but the rich variety of phases that exist at high pressure should provide a fertile playground to further study topology and its interplay with other phenomena.

## ACKNOWLEDGMENTS

This work was supported by National Natural Science Foundation of China (Grants No. 12274169, No. 12122405, and No. 52072188), National Key R&D Program of China (Grant No. 2022YFA1402304), the Program for Science and Technology Innovation Team in Zhejiang (Grant No. 2021R01004), and Jilin Provincial Science and Technology Development Project (Project No. 20210509038RQ). B.M. acknowledges support from a UKRI Future Leaders Fellowship [MR/V023926/1], from the Gianna Angelopoulos Programme for Science, Technology, and Innovation, and from the Winton Programme for the Physics of Sustainability. C.J.P. acknowledges financial support from the Engineering and Physical Sciences Research Council (Grant No. EP/P022596/1) and a Royal Society Wolfson Research Merit award. Parts of the calculations were performed in the High Performance Computing Center (HPCC) of Jilin University and TianHe-1(A) at the National Supercomputer Center in Tianjin. For the purpose of open access, the authors have applied a Creative Commons Attribution (CC BY) license to any author accepted manuscript version arising.

T.C. and D.D. initiated the project and carried out the theoretical analysis. Z.Z. performed the first-principles calculations and theoretical analysis. B.M. provided several key suggestions on high-pressure physics and topological materials. C.J.P. and H.S. performed the *ab initio* random structure searching. All authors contributed to the discussion and the final version of the manuscript.

The authors declare no competing interests.

- [1] L. Lu, L. Fu, J. D. Joannopoulos, and M. Soljačić, Weyl points and line nodes in gyroid photonic crystals, *Nat. Photon.* **7**, 294 (2013).  
 [2] N. Morali, R. Batabyal, P. K. Nag, E. Liu, Q. Xu, Y. Sun, B. Yan, C. Felser, N. Avraham, and H. Beidenkopf, Fermi-arc diversity on surface terminations of the magnetic Weyl semimetal  $\text{Co}_3\text{Sn}_2\text{S}_2$ , *Science* **365**, 1286 (2019).

- [3] T. Bzdusek, Q. Wu, A. Ruegg, M. Sigrist, and A. A. Soluyanov, Nodal-chain metals, *Nature (London)* **538**, 75 (2016).  
 [4] J. T. Wang, S. Nie, H. Weng, Y. Kawazoe, and C. Chen, Topological nodal-net semimetal in a graphene network structure, *Phys. Rev. Lett.* **120**, 026402 (2018).

- [5] C. Zhong, Y. Chen, Y. Xie, S. A. Yang, M. L. Cohen, and S. B. Zhang, Towards three-dimensional Weyl-surface semimetals in graphene networks, *Nanoscale* **8**, 7232 (2016).
- [6] S. Z. Chen, S. Li, Y. Chen, and W. Duan, Nodal flexible-surface semimetals: Case of carbon nanotube networks, *Nano Lett.* **20**, 5400 (2020).
- [7] Z. Wang, A. Alexandradinata, R. J. Cava, and B. A. Bernevig, Hourglass fermions, *Nature (London)* **532**, 189 (2016).
- [8] S. Ahn, E. J. Mele, and H. Min, Electrodynamics on fermi cyclides in nodal line semimetals, *Phys. Rev. Lett.* **119**, 147402 (2017).
- [9] J. Gooth, B. Bradlyn, S. Honnali, C. Schindler, N. Kumar, J. Noky, Y. Qi, C. Shekhar, Y. Sun, Z. Wang, B. A. Bernevig, and C. Felser, Axionic charge-density wave in the Weyl semimetal  $(\text{TaSe}_4)_2\text{I}$ , *Nature (London)* **575**, 315 (2019).
- [10] B. B. Fu, C. J. Yi, T. T. Zhang, M. Caputo, J. Z. Ma, X. Gao, B. Q. Lv, L. Y. Kong, Y. B. Huang, P. Richard, M. Shi, V. N. Strocov, C. Fang, H. M. Weng, Y. G. Shi, T. Qian, and H. Ding, Dirac nodal surfaces and nodal lines in  $\text{ZrSiS}$ , *Sci. Adv.* **5**, eaau6459 (2019).
- [11] W. Wu, Y. Liu, S. Li, C. Zhong, Z.-M. Yu, X.-L. Sheng, Y. X. Zhao, and S. A. Yang, Nodal surface semimetals: Theory and material realization, *Phys. Rev. B* **97**, 115125 (2018).
- [12] C. Song, L. Jin, P. Song, H. Rong, W. Zhu, B. Liang, S. Cui, Z. Sun, L. Zhao, Y. Shi, X. Zhang, G. Liu, and X. J. Zhou, Spectroscopic evidence for Dirac nodal surfaces and nodal rings in the superconductor  $\text{NaAlSi}$ , *Phys. Rev. B* **105**, L161104 (2022).
- [13] S. A. Mack, S. M. Griffin, and J. B. Neaton, Emergence of topological electronic phases in elemental lithium under pressure, *Proc. Natl. Acad. Sci. USA* **116**, 9197 (2019).
- [14] M. S. Bahramy, B. J. Yang, R. Arita, and N. Nagaosa, Emergence of non-centrosymmetric topological insulating phase in  $\text{BiTeI}$  under pressure, *Nat. Commun.* **3**, 679 (2012).
- [15] L. C. Chen, P. Q. Chen, W. J. Li, Q. Zhang, V. V. Struzhkin, A. F. Goncharov, Z. Ren, and X. J. Chen, Enhancement of thermoelectric performance across the topological phase transition in dense lead selenide, *Nature Mater.* **18**, 1321 (2019).
- [16] N. W. Ashcroft, Metallic hydrogen: A high-temperature superconductor? *Phys. Rev. Lett.* **21**, 1748 (1968).
- [17] N. W. Ashcroft, Hydrogen dominant metallic alloys: High temperature superconductors? *Phys. Rev. Lett.* **92**, 187002 (2004).
- [18] D. Duan, Y. Liu, F. Tian, D. Li, X. Huang, Z. Zhao, H. Yu, B. Liu, W. Tian, and T. Cui, Pressure-induced metallization of dense  $(\text{H}_2\text{S})_2\text{H}_2$  with high- $T_c$  superconductivity, *Sci. Rep.* **4**, 6968 (2014).
- [19] Z. Zhang, T. Cui, M. J. Hutcheon, A. M. Shipley, H. Song, M. Du, V. Z. Kresin, D. Duan, C. J. Pickard, and Y. Yao, Design principles for high-temperature superconductors with a hydrogen-based alloy backbone at moderate pressure, *Phys. Rev. Lett.* **128**, 047001 (2022).
- [20] I. I. Naumov and R. J. Hemley, Topological surface states in dense solid hydrogen, *Phys. Rev. Lett.* **117**, 206403 (2016).
- [21] K. Puhakainen, D. Benson, J. Nysten, S. Konar, E. Stoyanov, K. Leinenweber, and U. Häussermann, Hypervalent octahedral  $\text{SiH}_6^{2-}$  species from high-pressure synthesis, *Angew. Chem. Int. Ed.* **51**, 3156 (2012).
- [22] O. Y. Vekilova, D. C. Beyer, S. Bhat, R. Farla, V. Baran, S. I. Simak, H. Kohlmann, U. Häussermann, and K. Spektor, Formation and polymorphism of semiconducting  $\text{K}_2\text{SiH}_6$  and strategy for metallization, *Inorg. Chem.* **62**, 8093 (2023).
- [23] S. Klemenz, A. K. Hay, S. M. L. Teicher, A. Topp, J. Cano, and L. M. Schoop, The role of delocalized chemical bonding in square-net-based topological semimetals, *J. Am. Chem. Soc.* **142**, 6350 (2020).
- [24] J. F. Khoury, B. Han, M. Jovanovic, R. Singha, X. Song, R. Queiroz, N.-P. Ong, and L. M. Schoop, A class of magnetic topological material candidates with hypervalent Bi chains, *J. Am. Chem. Soc.* **144**, 9785 (2022).
- [25] L. Liu, C. Wang, S. Yi, K. W. Kim, J. Kim, and J.-H. Cho, Microscopic mechanism of room-temperature superconductivity in compressed  $\text{LaH}_{10}$ , *Phys. Rev. B* **99**, 140501(R) (2019).
- [26] C. Wang, S. Liu, H. Jeon, S. Yi, Y. Bang, and J.-H. Cho, Effect of hole doping on superconductivity in compressed  $\text{CeH}_9$  at high pressures, *Phys. Rev. B* **104**, L020504 (2021).
- [27] A. P. Drozdov, M. I. Erements, I. A. Troyan, V. Ksenofontov, and S. I. Shylin, Conventional superconductivity at 203 kelvin at high pressures in the sulfur hydride system, *Nature (London)* **525**, 73 (2015).
- [28] A. P. Drozdov, P. P. Kong, V. S. Minkov, S. P. Besedin, M. A. Kuzovnikov, S. Mozaffari, L. Balicas, F. F. Balakirev, D. E. Graf, V. B. Prakapenka, E. Greenberg, D. A. Knyazev, M. Tkacz, and M. I. Erements, Superconductivity at 250 K in lanthanum hydride under high pressures, *Nature (London)* **569**, 528 (2019).
- [29] H. Liu, I. I. Naumov, R. Hoffmann, N. W. Ashcroft, and R. J. Hemley, Potential high- $T_c$  superconducting lanthanum and yttrium hydrides at high pressure, *Proc. Natl. Acad. Sci. USA* **114**, 6990 (2017).
- [30] K. Spektor, W. A. Crichton, S. Filippov, S. I. Simak, A. Fischer, and U. Häussermann,  $\text{Na}_3\text{FeH}_7$  and  $\text{Na}_3\text{CoH}_6$ : Hydrogen-rich first-row transition metal hydrides from high pressure synthesis, *Inorg. Chem.* **59**, 16467 (2020).
- [31] J. Wang, Y. Liu, K. H. Jin, X. Sui, L. Zhang, W. Duan, F. Liu, and B. Huang, Pseudo Dirac nodal sphere semimetal, *Phys. Rev. B* **98**, 201112(R) (2018).
- [32] M. Hirayama, R. Okugawa, T. Miyake, and S. Murakami, Topological Dirac nodal lines and surface charges in fcc alkaline earth metals, *Nat. Commun.* **8**, 14022 (2017).
- [33] L. Yan, C. Ding, M. Li, R. Tang, W. Chen, B. Liu, K. Bu, T. Huang, D. Dai, X. Jin, X. Yang, E. Cheng, N. Li, Q. Zhang, F. Liu, X. Liu, D. Zhang, S. Ma, Q. Tao, P. Zhu, S. Li, X. Lü, J. Sun, X. Wang, and W. Yang, Modulating charge-density wave order and superconductivity from two alternative stacked monolayers in a bulk  $4\text{Hb-TaSe}_2$  heterostructure via pressure, *Nano Lett.* **23**, 2121 (2023).
- [34] B. Bradlyn, L. Elcoro, J. Cano, M. G. Vergniory, Z. J. Wang, C. Felser, M. I. Aroyo, and B. A. Bernevig, Topological quantum chemistry, *Nature (London)* **547**, 298 (2017).
- [35] F. Tang, H. C. Po, A. Vishwanath, and X. G. Wan, Efficient topological materials discovery using symmetry indicators, *Nat. Phys.* **15**, 470 (2019).
- [36] Z. Liu, H. Wang, Z. F. Wang, J. L. Yang, and F. Liu, Pressure-induced organic topological nodal-line semimetal in the three-dimensional molecular crystal  $\text{Pd}(\text{ddd})_2$ , *Phys. Rev. B* **97**, 155138 (2018).
- [37] See Supplemental Material at <http://link.aps.org/supplemental/10.1103/PhysRevB.108.205119> for band structure and phonon dispersion of supervalent hydrides  $A_2\text{BH}_6$  ( $A = \text{Mg}^{2+}, \text{Ca}^{2+}$ ,

- $\text{Sr}^{2+}$ ,  $\text{Ba}^{2+}$ , and  $B = \text{Be}^{2+}$ ,  $\text{Zn}^{2+}$ ,  $\text{Cu}^{2+}$ ) with symmetry  $Fm - 3m$ , CDW caused by a lattice instability in  $\text{Mg}_2\text{BeH}_6$  ( $R\bar{3}$ ), topological charge of  $\text{Mg}_2\text{BeH}_6$  ( $Fm - 3m$ ), the response of fermions in  $\text{Mg}_2\text{BeH}_6$  ( $Fm - 3m$ ), computational details, and structural parameters. It also contains Refs. [11,38–56].
- [38] C. J. Pickard and R. J. Needs, *Ab initio* random structure searching, *J. Phys.: Condens. Matter* **23**, 053201 (2011).
- [39] Z. Wang, Y. Yao, L. Zhu, H. Liu, T. Iitaka, H. Wang, and Y. Ma, Metallization and superconductivity of  $\text{BeH}_2$  under high pressure, *J. Chem. Phys.* **140**, 124707 (2014).
- [40] D. C. Lonie, J. Hooper, B. Altintas, and E. Zurek, Metallization of magnesium polyhydrides under pressure, *Phys. Rev. B* **87**, 054107 (2013).
- [41] A. P. Schnyder, S. Ryu, A. Furusaki, and A. W. W. Ludwig, Classification of topological insulators and superconductors in three spatial dimensions, *Phys. Rev. B* **78**, 195125 (2008).
- [42] O. TÜRker and S. Moroz, Weyl nodal surfaces, *Phys. Rev. B* **97**, 075120 (2018).
- [43] M. D. Segall, P. J. D. Lindan, M. J. Probert, C. J. Pickard, P. J. Hasnip, S. J. Clark, and M. C. Payne, First-principles simulation: Ideas, illustrations and the CASTEP code, *J. Phys.: Condens. Matter* **14**, 2717 (2002).
- [44] G. Kresse and D. Joubert, From ultrasoft pseudopotentials to the projector augmented-wave method, *Phys. Rev. B* **59**, 1758 (1999).
- [45] G. Kresse and J. Furthmüller, Efficiency of ab-initio total energy calculations for metals and semiconductors using a plane-wave basis set, *Comput. Mater. Sci.* **6**, 15 (1996).
- [46] J. P. Perdew, K. Burke, and Y. Wang, Generalized gradient approximation for the exchange-correlation hole of a many-electron system, *Phys. Rev. B* **54**, 16533 (1996).
- [47] J. P. Perdew and Y. Wang, Accurate and simple analytic representation of the electron-gas correlation energy, *Phys. Rev. B* **45**, 13244 (1992).
- [48] A. D. Becke and K. E. Edgecombe, A simple measure of electron localization in atomic and molecular systems, *J. Chem. Phys.* **92**, 5397 (1990).
- [49] G. Henkelman, A. Arnaldsson, and H. Jónsson, A fast and robust algorithm for Bader decomposition of charge density, *Comput. Mater. Sci.* **36**, 354 (2006).
- [50] W. Tang, E. Sanville, and G. Henkelman, A grid-based Bader analysis algorithm without lattice bias, *J. Phys.: Condens. Matter* **21**, 084204 (2009).
- [51] Q. Wu, S. Zhang, H.-F. Song, M. Troyer, and A. A. Soluyanov, WannierTools: An open-source software package for novel topological materials, *Comput. Phys. Commun.* **224**, 405 (2018).
- [52] A. A. Mostofi, J. R. Yates, Y. S. Lee, I. Souza, D. Vanderbilt, and N. Marzari, wannier90: A tool for obtaining maximally-localised Wannier functions, *Comput. Phys. Commun.* **178**, 685 (2008).
- [53] I. Souza, N. Marzari, and D. Vanderbilt, Maximally localized Wannier functions for entangled energy bands, *Phys. Rev. B* **65**, 035109 (2001).
- [54] A. Togo, L. Chaput, T. Tadano, and I. Tanaka, Implementation strategies in phonopy and phono3py, *J. Phys.: Condens. Matter* **35**, 353001 (2023).
- [55] P. Giannozzi, S. Baroni, N. Bonini, M. Calandra, R. Car, C. Cavazzoni, D. Ceresoli, G. L. Chiarotti, M. Cococcioni, I. Dabo, A. Dal Corso, S. De Gironcoli, S. Fabris, G. Fratesi, R. Gebauer, U. Gerstmann, C. Gougoussis, A. Kokalj, M. Lazzeri, L. Martin-Samos *et al.*, QUANTUM ESPRESSO: A modular and open-source software project for quantum simulations of materials, *J. Phys.: Condens. Matter* **21**, 395502 (2009).
- [56] W. L. McMillan, Transition temperature of strong-coupled superconductors, *Phys. Rev.* **167**, 331 (1968).
- [57] S. Shao, J.-X. Yin, I. Belopolski, J.-Y. You, T. Hou, H. Chen, Y. Jiang, M. S. Hossain, M. Yahyavi, C.-H. Hsu, Y. P. Feng, A. Bansil, M. Z. Hasan, and G. Chang, Intertwining of magnetism and charge ordering in kagome FeGe, *ACS Nano* **17**, 10164 (2023).
- [58] W. Kohn, Image of the fermi surface in the vibration spectrum of a metal, *Phys. Rev. Lett.* **2**, 393 (1959).
- [59] A. V. Lugovskoi, M. I. Katsnelson, and A. N. Rudenko, Strong electron-phonon coupling and its influence on the transport and optical properties of hole-doped single-layer InSe, *Phys. Rev. Lett.* **123**, 176401 (2019).
- [60] R. Li, J. Li, L. Wang, J. Liu, H. Ma, H.-F. Song, D. Li, Y. Li, and X.-Q. Chen, Underlying topological dirac nodal line mechanism of the anomalously large electron-phonon coupling strength on a Be (0001) surface, *Phys. Rev. Lett.* **123**, 136802 (2019).